NANO LETTERS

Letter

pubs.acs.org/NanoLett

Crystallization of Amphiphilic DNA C-Stars

Ryan A. Brady,[†] Nicholas J. Brooks,[‡] Pietro Cicuta,*[,†] and Lorenzo Di Michele*[,†]

[†]Biological and Soft Systems, Cavendish Laboratory, University of Cambridge, Cambridge CB3 0HE, U.K.

[‡]Department of Chemistry, Imperial College London, London SW7 2AZ, U.K.

Supporting Information

ABSTRACT: Many emerging technologies require materials with well-defined three-dimensional nanoscale architectures. Production of these structures is currently underpinned by self-assembling amphiphilic macromolecules or engineered all-DNA building blocks. Both of these approaches produce restricted ranges of crystal geometries due to synthetic amphiphiles' simple shape and limited specificity, or the technical difficulties in designing space-filling DNA motifs with targeted shapes. We have overcome these limitations with amphiphilic DNA nanostructures, or "C-Stars", that combine the design freedom and facile functionalization of DNA-based materials with robust hydrophobic interactions. C-Stars self-assemble into single crystals exceeding 40 μm in size with lattice parameters exceeding 20 nm.

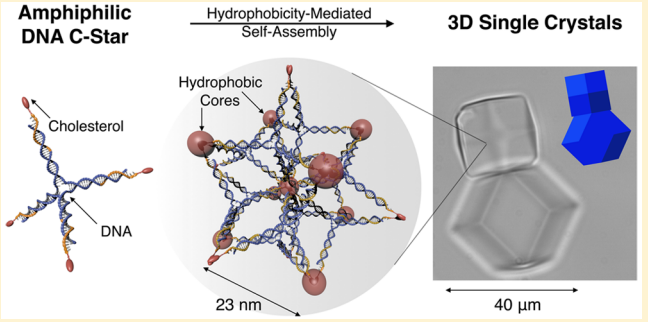

KEYWORDS: *DNA crystallization, hydrophobic interactions, amphiphilic molecules, self-assembly, single crystals, DNA nanotechnology*

The pressing need for materials with a controlled and regular nanostructure calls for the development of reliable self-assembly methods, where engineered nanoscale units spontaneously aggregate into ordered arrays. DNA has emerged as the component of choice to produce building blocks of arbitrary shape and functionality.[1−5] Branched junctions that interact through single-stranded overhangs are the simplest DNA nanostructures capable of forming a network connected specifically by base pairing. Such "nanostars" were the first DNA-based units proposed for self-assembled ordered materials,[6,7] but were found unsuitable as their flexibility instead leads to the formation of disordered hydrogels.[8−11] Subsequent attempts confirmed that efficient three-dimensional (3D) crystallization requires DNA nanostructures with high structural rigidity and precise bond directionality.[5] Indeed, following these guidelines, Seeman and co-workers devised a tensegrity triangle DNA motif capable of sustaining periodicity.[12−15] This breakthrough enabled the construction of macroscopic single crystals achieving a remarkable assembly accuracy, exceeding 4 Å. Based on the same design principles, the authors recently produced slight variations of the original motif.[16] Yet, the few identified by Seeman and co-workers remain to date the only examples of all-DNA nanostructures shown to form 3D crystals; a very surprising occurrence particularly in view of the virtually unlimited design space. This apparent lack of versatility hints at the intrinsic difficulties that one may encounter when trying to devise a rigid and space-filling DNA unit. Indeed, 3D crystallization requires the formation of bonds with very precise orientations, compatible with the targeted lattice symmetry. The stiffness of double-stranded (ds)DNA at the molecular scale introduces constraints on the exact orientation of specific features, which massively narrow down the design space and make the search for suitable architectures a formidable task.

Stiff building blocks interacting via rigid lock-and-key molecular bonds are essential for achieving the subnanometer self-assembly accuracy required, for instance, if one aims to use the DNA scaffolds to template protein crystallization for diffraction studies.[17] However, many other applications including sensing,[18−20] photonics,[21] energy storage,[22,23] catalysis,[24] and molecular sieving[25] do not require Angstrom precision and would greatly benefit from a more versatile approach to bulk DNA self-assembly, capable of expanding the range of available crystal structures.

Amphiphilic molecules exhibit a natural tendency to support long-range order in one, two, and three dimensions, making them ubiquitous structural elements in Biology and artificial materials.[26−29] Examples of 3D crystals include lipids forming exotic cubic phases[26,29,30] and synthetic diblock copolymers self-assembling into bicontinuous gyroid phases.[27,28,31−33] Strikingly, in these materials macroscopic periodicity does not arise from a regular arrangement at the single-molecule level. Instead, lipids and block copolymers are locally disordered, and crystallinity only emerges from the frustrated phase separation of hydrophobic and hydrophilic domains at a mesoscopic scale. However, despite the indisputable robustness of this self-assembly principle, the simple shape and limited tailorability of

Received: March 7, 2017
Revised: April 17, 2017
Published: April 18, 2017

DOI: 10.1021/acs.nanolett.7b00980
Nano Lett. 2017, 17, 3276−3281

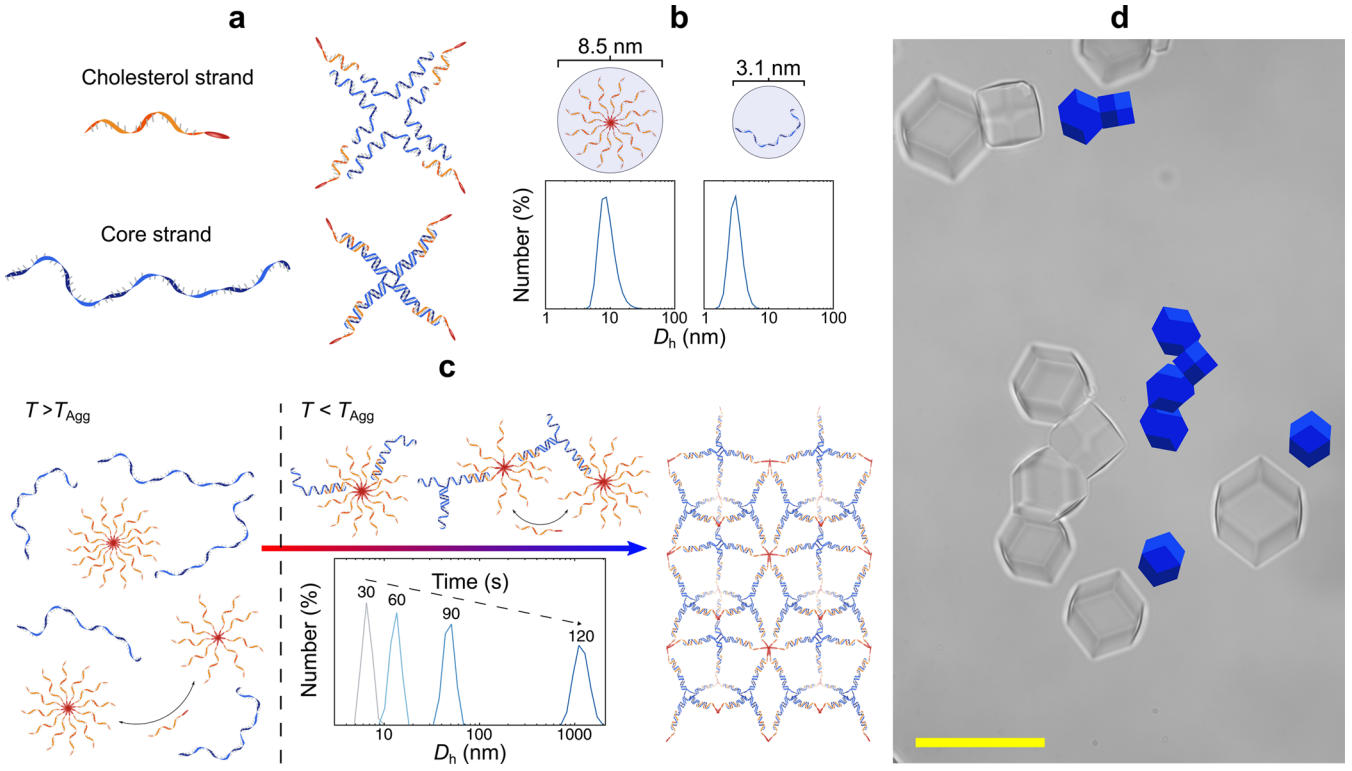

Figure 1. Design and self-assembly of crystal-forming amphiphilic DNA nanostructures. (a) Amphiphilic DNA-nanostars (C-Stars) with four arms self-assemble from four different oligonucleotides forming the C-Star core and four identical cholesterol-functionalized strands providing amphiphilic character. (b) Dynamic light scattering (DLS) indicates that cholesterol-functionalized strands form micelles with hydrodynamic diameter of 8.5 ± 1.5 nm. Isolated core strands display hydrodynamic diameter of 3.1 ± 0.4 nm. (c) Self-assembly pathway for C-Stars. Cholesterol-functionalized strands and core strands are mixed in stoichiometric ratio. At high temperature (left) micelles coexists with single-stranded core strands. When temperature is reduced below T_{Agg} = 77.1 ± 0.2 °C (center), C-Star cores begin to form and bridge together existing micelles, which adjust their size to accommodate the coordination imposed by the nanostar motifs. Aggregates nucleate and grow over time, as demonstrated by DLS (inset), forming extended crystalline networks (right). Here we reproduce the (100) crystallographic plane of the structure shown in Figure 2. (d) When cooled slowly from above T_{Agg}, C-Stars form well-defined single crystal-shape-like rhombic dodecahedra, shown in bright field optical images. In blue we show model rhombic dodecahedra with the same orientation of nearby crystallites. Scale bar: 50 μm.

the molecular units significantly constrains the accessible range of crystal structures, their lattice parameter, and their porosity.

Here, we combine the design versatility of DNA nanotechnology with the robustness of hydrophobic interactions to create amphiphilic DNA nanostructures, which we name "C-Stars". These can reliably self-assemble into macroscopic single crystals exceeding 40 μm and 10^{10} building blocks in size. As sketched in Figure 1a, C-Stars are flexible junctions featuring n = 4 arms, similar to the earliest DNA building blocks devised. However, rather than terminating in an unpaired single-stranded DNA (ssDNA) overhang,[9,10] here each arm ends with a cholesterol molecule, which grants the structures amphiphilic character. In contrast to conventional all-DNA building blocks, C-Stars do not have a fixed valency of binding, as their aggregation is supported by multiple hydrophobic modifications segregating into dense micelle-like clusters, which provide structural rigidity. The flexible DNA motifs connect the micelles, controlling their arrangement in space and ultimately determining the crystal structure. In this context, a strict control over the 3D geometry of the DNA building blocks is no longer required, lifting the design constraints that have been hampering the diversification of all-DNA crystals. What controls the nanophase separation between hydrophilic and hydrophobic segments is indeed the C-Star topology, which can be designed easily and precisely.

C-Stars are prepared from four different "core" single-strands, whose nucleotide sequence imposes the star-shape, and four identical cholesterol-functionalized strands complementary to part of the core strands (Figure 1a). To confer additional flexibility, single unpaired *A* bases are left to separate each arm at the central junction, and two unpaired *A* bases and a triethylene glycol spacer are used to connect the cholesterol to the end of each double-stranded DNA (dsDNA) arm, which also feature a nick halfway along their length. Cholesterol functionalized strands are themselves amphiphilic and, in the absence of core strands, form micelles with a hydrodynamic diameter of 8.5 ± 1.5 nm, corresponding to 5−16 strands per micelle (Figure 1b, see Theoretical Calculations in SI). We prepared C-Star samples where all the single-stranded components are mixed in stoichiometric ratio, with an overall C-Star concentration of 5 μM. At high temperatures ($T > T_{Agg}$ = 77.1 ± 0.2 °C) cholesterol−DNA micelles coexist with free core strands as sketched in Figure 1c. Upon slow quenching, as the temperature crosses T_{Agg}, we observe a phase transition, where aggregates nucleate and grow rapidly (Figure 1c, inset). Aggregation is triggered by the self-assembly of the C-Star cores mediated by Watson−Crick base pairing, which cross-link existing micelles and lead to the formation of a crystalline network. At this stage the micelles will adapt their size to meet the structural constraints imposed by the C-Star motifs, until all DNA−DNA bonds are formed and the micelles become

DOI: 10.1021/acs.nanolett.7b00980
Nano Lett. 2017, 17, 3276−3281

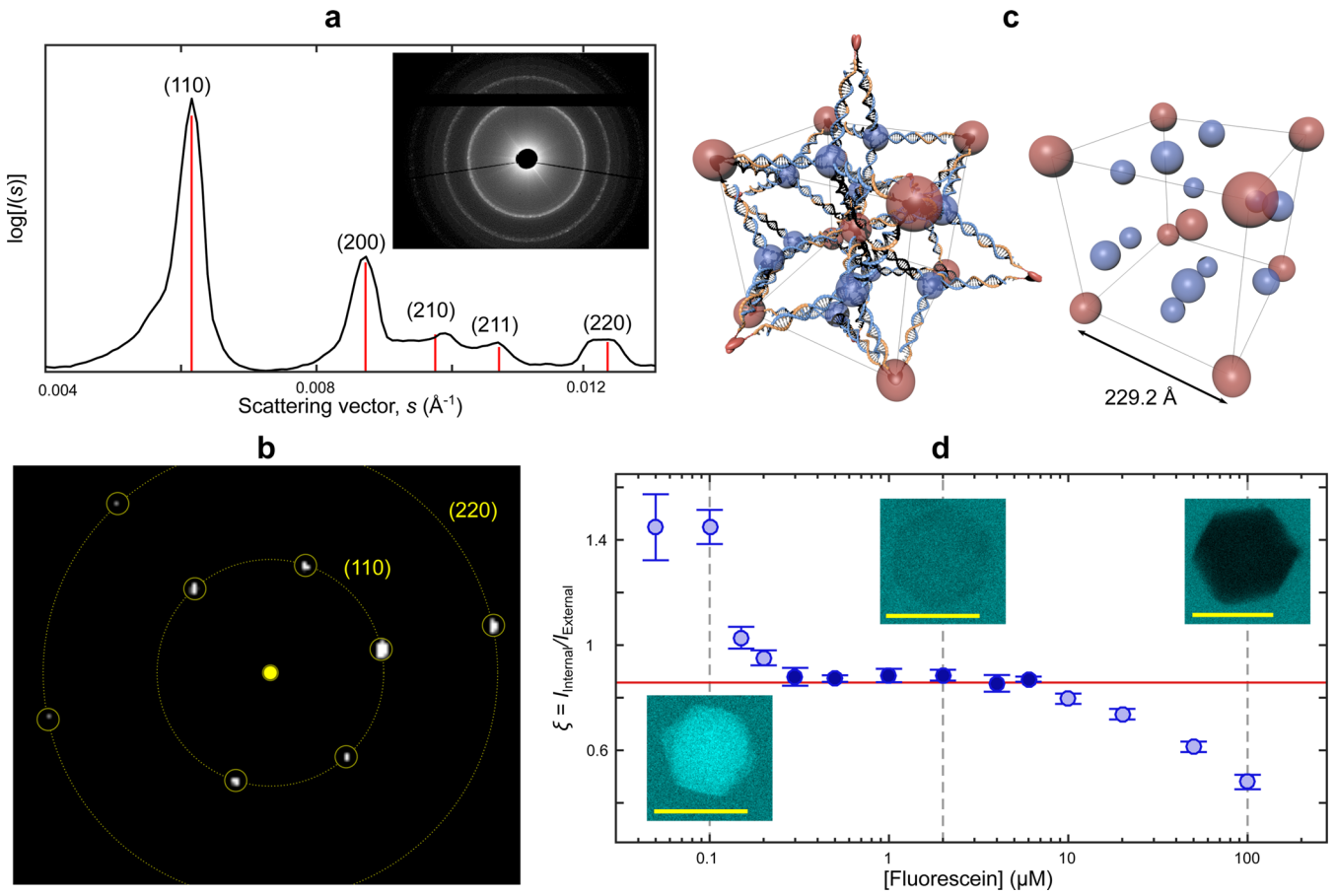

Figure 2. Microstructure and porosity of four-pointed C-Star crystals. (a) SAXS powder diffraction pattern (inset) and radial intensity profile (black solid line) for a dense sample of C-Star crystals. Red vertical lines indicate the best fit of the pattern to the Bragg peaks of a cubic lattice with $Pm\bar{3}n$ or a $P\bar{4}3n$ space group. Fitted lattice parameter: 229.2 Å. (b) Single-crystal diffraction pattern obtained by illuminating individual crystals within the sample with a narrowly focused X-ray beam. Circles highlight diffraction spots in locations compatible with a BCC lattice. (c) Plausible arrangement of C-Stars within a $Pm\bar{3}n$ unit cell. C-Star junctions are located on two lattice points on each face of the unit cube. Cholesterol functionalized arms extend toward the center or the vertices of the cube, forming an array of micelles with a body-center cubic symmetry. Micelles and C-Star junctions are highlighted by red and blue spheres, clearly visible on the left-hand-side diagram, where C-Stars are not shown. (d) Fluorescein permeation quantified by the ratio ξ between the fluorescent intensity measured inside and outside crystallites for varying concentration of fluorescein sodium salt. Intensity is evaluated from confocal microscopy images, examples of which are shown in the insets. Scale bars are 20 μm. The horizontal red line marks the expected value of ξ, estimated assuming the unit cell shown in panel c as discussed in the SI.

monodisperse (see Figure 1c). This adaptation is thermodynamically driven by the strength of DNA connections, whose binding free energy exceeds 45 k_BT at room temperature.[34] Exchange of cholesterol−DNA strands between micelles is kinetically favored by the dynamic nature of these aggregates.[35,36]

Figure 1d shows equilibrium single crystals, or Wulff polyhedra, obtained after slowly cooling samples from 95 to 30 °C at a rate of −0.01 °C min^{-1}.[37] Comparison with model polyhedra reveals how nearly all crystallites have the shape of a rhombic dodecahedron, a Wulff polyhedron associated with a cubic unit cell, whose facets correspond to (110) crystallographic planes. Crystallization of C-Stars is carried out in Tris-EDTA buffer with an additional 300 mM NaCl, without the need of divalent ions typically added in high concentration to stabilize more complex DNA architectures,[1−4] including those successfully crystallized by Seeman and co-workers.[12−14] See SI for detailed Experimental Methods and Expanded Discussion of C-Star design and aggregation.

The microscopic crystal structure is assessed by synchrotron-based small angle X-ray scattering (SAXS). The "powder" diffraction pattern in Figure 2b is recorded on concentrated samples of closely packed crystals obtained by sedimentation and clearly exhibits bright Bragg peaks, unambiguously demonstrating the crystalline nature of the material. Four of these peaks are consistent with the (110), (200), (210), and (220) reflections of a simple body-centered cubic (BCC) unit cell with a lattice parameter of 229.2 Å, and a fifth peak is aligned with a (211) reflection. This suggests a $Pm\bar{3}n$ or a $P\bar{4}3n$ symmetry unit cell, with the apparent slight variation from ideal peak positions that could be caused by small impurities of another structure or deformations, which are also likely to be the cause of the broadening of the (220) peak. Additionally, microfocus X-ray diffraction (with a spot size of 10 μm) was used to probe individual crystals of the DNA nanostructure. The recorded single-crystal diffraction patterns, an example of which is shown in Figure 2c, confirm a BCC symmetry (see SI Figure S2 for additional patterns). This symmetry is also consistent with the 3D shape of the Wulff polyhedra, as BCC crystals often form rhombic dodecahedral crystallites enclosed by (110) crystallographic planes.[38] The dense micelle-like hydrophobic cores can be assumed as the main sources of

DOI: 10.1021/acs.nanolett.7b00980
Nano Lett. 2017, 17, 3276−3281

scattering, thus one can attempt to reconstruct the arrangement of the C-Stars in a cubic unit cell where hydrophobic moieties converge toward the lattice points of a BCC. Figure 2c shows a plausible geometry featuring six C-Stars per unit cell and 12 cholesterol molecules converging onto each BCC site (red beads). C-Star junctions are placed on lattice points on the faces of the unit cube (blue beads), where they are equidistant from exactly four micellar sites, elucidating how the C-Star topology dictates the spatial arrangement of the micelles. This structural arrangement is compatible with a $Pm\bar{3}n$ space group, explaining the (211) reflection observed in the powder diffraction pattern. Furthermore, with this arrangement, the measured lattice parameter is in good agreement with the size of the C-Stars. The number of cholesterol molecules per hydrophobic core is also compatible with that in micelles formed by freely diffusing cholesterol-functionalized strands, estimated in the range 5−16 from DLS measurements of hydrodynamic radius after modeling the micelles as star polymers[39] (Figure 1b, see Theoretical Calculations in SI). We also note that a $Pm\bar{3}n$ lattice, indicated as A15, has been observed in dense aggregates of repulsive micelles in soap froths.[40] Finally, our interpretation of the C-Star arrangement, with the formation of hydrophobic cores cross-linked by the nanostars, is supported by *in silico* observations of amphiphilic star polymers with rigid[41] and flexible arms.[42]

To complete the structural characterization of C-Star crystals we perform a porosity assay using fluorescein permeation. Crystals are incubated in solutions with varying concentration of fluorescein sodium salt, then the permeation of the fluorophore is deduced in confocal microscopy experiments by measuring the ratio ξ between the fluorescence intensity recorded within the crystals ($I_{internal}$) and in the surrounding free space ($I_{external}$). Results are summarized in Figure 2d. At very low fluorescein concentration we observe a preferential partitioning of the fluorescein within the crystals, possibly due to a slight hydrophobicity of the fluorophores, finding favorable binding sites in correspondence with the cholesterol-rich regions. Upon increasing fluorescein concentration, the intensity ratio plateaus at $\xi \approx 0.84$ and remains constant, indicating free diffusion of the fluorophores within the DNA network. In this regime, ξ is equal to the fraction of free volume available to fluorophores within a unit cell $V_{free}/V_{uc} = 1-V_{exc}/V_{uc}$, where V_{uc} is the volume of the unit cell and V_{exc} is the excluded volume caused by the presence of the C-Star network. Assuming the unit-cell structure deduced by SAXS data, approximating dsDNA helices as charged cylinders of radius 10 Å and fluorescein ions as spheres of radius 5 Å, we could estimate the fraction of free volume available to fluorophores within the crystals, shown as a red line in Figure 2d (see Theoretical Calculations, SI). The agreement with the experimental observations is remarkable, further supporting our description of the internal structure of C-Star crystals. At much higher fluorescein concentrations, we observe a progressive drop of ξ, probably due to excessive Coulomb repulsion caused by the strong negative charge of DNA and fluorescein ions.

To assess how simple design variations affect self-assembly behavior we tested C-Stars with a different number of arms, namely, $n = 3$ and 6, shown in Figure 3. Optical microscopy examination evidenced macroscopic crystallites for both $n = 3$ and 6, similar in shape to those observed for $n = 4$. The morphology of $n = 3$ crystals is, however, more irregular, while samples of $n = 6$ C-Stars often produce more "rounded"

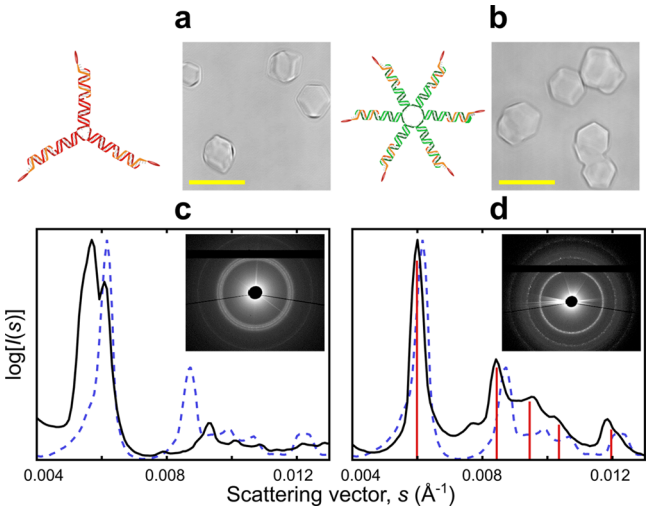

Figure 3. Macroscopic behavior and crystal structure depend on C-Star geometry. (a,b) Bright field images of aggregates formed by C-Stars with $n = 3$ and $n = 6$ arms (respectively). Scale bars are 20 μm. (c,d) SAXS powder diffraction patterns (insets) and radial intensity profiles (black solid lines) for $n = 3$ and $n = 6$ samples. The radial intensity profile for the $n = 4$ sample (dashed blue line) is overlaid for easier visual comparison. For $n = 6$ stars, the red vertical lines indicate the best fit to the diffraction pattern of a $Pm\bar{3}n$ or a $P\bar{4}3n$ space group.

aggregates, hinting at possible microscopic differences in the arrangement of C-Stars with different number of arms.

SAXS demonstrates the crystallinity of both samples of three-pointed and six-pointed C-Stars. Visual comparison between SAXS patterns confirms how C-Stars with different n crystallize differently. For three-pointed stars the SAXS pattern displays three overlapping major peaks indicating either coexistence of multiple cubic phases or a lower-symmetry unit cell. The latter scenario would be compatible with the observation of elongated crystallites. The lack of strong reflections at larger values of the scattering vector s indicates a less robust long-range order and makes it impossible to speculate on possible space groups. SAXS patterns of six-pointed stars are more similar to those of samples with $n = 4$, with the presence of the five reflections already observed in the latter, indicating a cubic unit cell with lattice parameter of 236.8 Å. The small peak at $s = 0.0076$ Å^{-1}, however, is not observed in $n = 4$ constructs hinting at different space group or a deformation of the cubic cell.

Roh et al. explored the use of amphiphilic DNA nanostructures for drug and gene delivery applications and proposed a design similar in shape to the three-pointed C-Stars, but featuring a single lipid modification rather than three cholesterol molecules.[43] These authors observed the formation of amorphous aggregates with an apparent core−shell structure, rather than crystalline lattices as in our case, further confirming how changes in building block design can heavily affect the self-assembly behavior.

The phase diagram in Figure 4 highlights the gas-crystal coexistence region for the three types of C-Stars. In comparison with conventional nanostars interacting through DNA overhangs,[10] C-Stars display a much wider coexistence region, reflecting the stronger interactions driving aggregation and the higher valency.[44] A re-entrance is observed for all C-Star designs in the temperature dependence of the aggregate density that displays a maximum at 70 °C, marking the onset of crystallization.[45] The density of the crystals has a clear dependence on the number of arms, with $n = 3$ samples

DOI: 10.1021/acs.nanolett.7b00980
Nano Lett. 2017, 17, 3276−3281

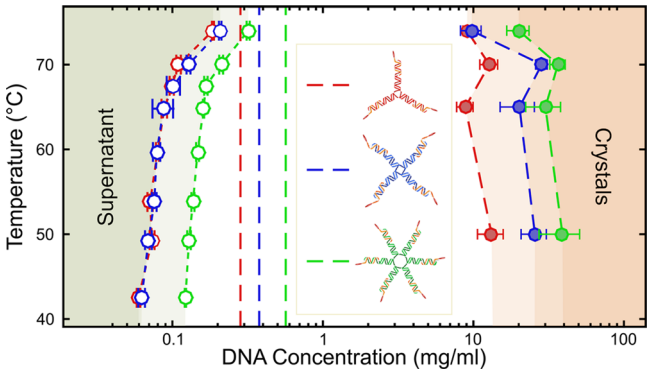

Figure 4. Phase behavior of C-Stars. Filled and empty symbols indicate the density of DNA within the aggregates and the surrounding supernatants, respectively, as measured via confocal-based fluorimetry and UV absorbance at various temperatures. Vertical dashed lines indicate the overall DNA mass concentration in the samples, corresponding to a molar concentration of 5 μM.

forming more "empty" aggregates and n = 6 more packed networks. This demonstrates how design changes, made easy by the full tailorability of DNA nanostructures, can be used to tune the physical properties of the aggregates.

Our results demonstrate how very simple and flexible DNA nanostructures, made amphiphilic by cholesterol moieties, reliably self-assemble into ordered phases forming large single crystals. Nanostructured crystalline materials are pivotal for a wide range of applications including sensing,[18−20] photonics,[21] energy storage,[22,23] and molecular sieving.[25] In addition, protocols exist to mineralize DNA networks, which can be applied to prepare nanoporous inorganics.[46] The use of DNA as the main reagent grants the additional advantages of facile handing, environmentally friendly synthesis, vast possibility of molecular functionalization,[15] and biocompatibility. Even though C-Stars interact via nonspecific hydrophobic forces, we demonstrate how features of the emergent crystals depend on nanostar design, specifically on the number of cholesterol-functionalized arms.

The applicability of our self-assembly principle is not restricted to the specific architectures discussed here. Since crystallization of DNA amphiphiles does not require rigidly prescribed building-block shapes as for all-DNA motifs, possible design variations are virtually unlimited and include changing arm length to tune lattice parameters and creating asymmetric motifs to access noncubic space groups, just to mention the most straightforward options. Moreover, DNA can be functionalized with a vast range of hydrophobic tags with different size and hydrophobicity, offering yet another designable feature to be explored.

Given the robustness and generality of the principles underlying our approach, we foresee it may develop into a general route for the production of macromolecular, nanostructured crystalline materials.

■ ASSOCIATED CONTENT

Supporting Information

The Supporting Information is available free of charge on the ACS Publications website at DOI: 10.1021/acs.nanolett.7b00980.

Experimental methods; expanded discussion; theoretical calculations; single crystal diffraction patters for n = 4 C-Stars (PDF)

■ AUTHOR INFORMATION

Corresponding Authors

*E-mail: pc245@cam.ac.uk.
*E-mail: ld389@cam.ac.uk.

ORCID

Pietro Cicuta: 0000-0002-9193-8496
Lorenzo Di Michele: 0000-0002-1458-9747

Notes

The authors declare no competing financial interest.

■ ACKNOWLEDGMENTS

L.D.M., P.C., and N.J.B. acknowledge support from the EPSRC Programme Grant CAPITALS number EP/J017566/1. L.D.M. acknowledges support from the Oppenheimer Fund, Emmanuel College Cambridge, the Leverhulme Trust, and the Isaac Newton Trust through an Early Career Fellowship (ECF-2015-494). R.A.B. acknowledges support from the EPSRC CDT in Nanoscience and Nanotechnology (NanoDTC), grant number EP/L015978/1. We acknowledge Diamond Light Source for provision of synchrotron beamtime (SM14217, SM15530, and SM15030), and we would like to thank Andy Smith for assistance in operating beamline I22. We thank Tuomas Knowles and Bortolo Mognetti for insightful discussions on this project. A complete dataset in support of this publication is available free of charge at https://doi.org/10.17863/CAM.9031.

■ REFERENCES

(1) Rothemund, P. W. K. *Nature* **2006**, *440*, 297−302.
(2) Iinuma, R.; Ke, Y.; Jungmann, R.; Schlichthaerle, T.; Woehrstein, J. B.; Yin, P. *Science* **2014**, *344*, 65−69.
(3) Ke, Y.; Ong, L. L.; Shih, W. M.; Yin, P. *Science* **2012**, *338*, 1177−1183.
(4) Tian, Y.; Wang, T.; Liu, W.; Xin, H. L.; Li, H.; Ke, Y.; Shih, W. M.; Gang, O. *Nat. Nanotechnol.* **2015**, *10*, 637−644.
(5) Jones, M. R.; Seeman, N. C.; Mirkin, C. A. *Science* **2015**, *347*, 1260901.
(6) Seeman, N. C. *J. Theor. Biol.* **1982**, *99*, 237−247.
(7) Seeman, N. C. *J. Biomol. Struct. Dyn.* **1985**, *3*, 11−34.
(8) Lee, J. B.; Peng, S.; Yang, D.; Roh, Y. H.; Funabashi, H.; Park, N.; Rice, E. J.; Chen, L.; Long, R.; Wu, M.; Luo, D. *Nat. Nanotechnol.* **2012**, *7*, 816−820.
(9) Um, S. H.; Lee, J. B.; Park, N.; Kwon, S. Y.; Umbach, C. C.; Luo, D. *Nat. Mater.* **2006**, *5*, 797−801.
(10) Biffi, S.; Cerbino, R.; Bomboi, F.; Paraboschi, E. M.; Asselta, R.; Sciortino, F.; Bellini, T. *Proc. Natl. Acad. Sci. U. S. A.* **2013**, *110*, 15633−15637.
(11) Rovigatti, L.; Smallenburg, F.; Romano, F.; Sciortino, F. *ACS Nano* **2014**, *8*, 3567−3574.
(12) Zheng, J.; Birktoft, J. J.; Chen, Y.; Wang, T.; Sha, R.; Constantinou, P. E.; Ginell, S. L.; Mao, C.; Seeman, N. C. *Nature* **2009**, *461*, 74−77.
(13) Sha, R.; Birktoft, J. J.; Nguyen, N.; Chandrasekaran, A. R.; Zheng, J.; Zhao, X.; Mao, C.; Seeman, N. C. *Nano Lett.* **2013**, *13*, 793−797.
(14) Wang, T.; Sha, R.; Birktoft, J.; Zheng, J.; Mao, C.; Seeman, N. C. *J. Am. Chem. Soc.* **2010**, *132*, 15471−15473.
(15) Hao, Y.; Kristiansen, M.; Sha, R.; Birktoft, J. J.; Hernandez, C.; Mao, C.; Seeman, N. C. *Nat. Chem.* **2017**, DOI: 10.1038/nchem.2745.
(16) Simmons, C. R.; Zhang, F.; Birktoft, J. J.; Qi, X.; Han, D.; Liu, Y.; Sha, R.; Abdallah, H.; Hernandez, C.; Ohayon, Y.; Seeman, N. C.; Yan, H. *J. Am. Chem. Soc.* **2016**, *138*, 10047−10054.
(17) Seeman, N. C. *Nature* **2004**, *421*, 427−431.
(18) Huang, X.-J.; Choi, Y.-K. *Sens. Actuators, B* **2007**, *122*, 659−671.

DOI: 10.1021/acs.nanolett.7b00980
Nano Lett. 2017, 17, 3276−3281

(19) Xia, L.; Wei, Z.; Wan, M. *J. Colloid Interface Sci.* **2010**, *341*, 1−11.
(20) Jimenez-Cadena, G.; Riu, J.; Rius, F. X. *Analyst* **2007**, *132*, 1083−1099.
(21) Flory, F.; Escoubas, L.; Berginc, G. *J. Nanophotonics* **2011**, *5*, 052502.
(22) Aricò, A. S.; Bruce, P.; Scrosati, B.; Tarascon, J.-M.; van Schalkwijk, W. *Nat. Mater.* **2005**, *4*, 366−377.
(23) Zhang, Q.; Uchaker, E.; Candelaria, S. L.; Cao, G. *Chem. Soc. Rev.* **2013**, *42*, 3127−3171.
(24) Ying, J. Y. *AIChE J.* **2000**, *46*, 1902−1906.
(25) Han, J.; Fu, J.; Schoch, R. B. *Lab Chip* **2008**, *8*, 23−33.
(26) Kulkarni, C. V. *Nanoscale* **2012**, *4*, 5779−5791.
(27) Mai, Y.; Eisenberg, A. *Chem. Soc. Rev.* **2012**, *41*, 5969−5985.
(28) Hu, H.; Gopinadhan, M.; Osuji, C. O. *Soft Matter* **2014**, *10*, 3867−3889.
(29) Luzzati, V. *Curr. Opin. Struct. Biol.* **1997**, *7*, 661−668.
(30) Seddon, A. M.; Curnow, P.; Booth, P. J. *Biochim. Biophys. Acta, Biomembr.* **2004**, *1666*, 105−117.
(31) Stefik, M.; Guldin, S.; Vignolini, S.; Wiesner, U.; Steiner, U. *Chem. Soc. Rev.* **2015**, *44*, 5076−5091.
(32) Hajduk, D. A.; Harper, P. E.; Gruner, S. M.; Honeker, C. C.; Kim, G.; Thomas, E. L.; Fetters, L. J. *Macromolecules* **1994**, *27*, 4063−4075.
(33) Chan, V. Z.-H.; Hoffman, J.; Lee, V. Y.; Iatrou, H.; Avgeropoulos, A.; Hadjichristidis, N.; Miller, R. D.; Thomas, E. L. *Science* **1999**, *286*, 1716−1719.
(34) SantaLucia, J. *Proc. Natl. Acad. Sci. U. S. A.* **1998**, *95*, 1460−1465.
(35) Choi, K.-m.; Kwon, I. C.; Ahn, H. J. *Biomaterials* **2013**, *34*, 4183−4190.
(36) Pfeiffer, I.; Höök, F. *J. Am. Chem. Soc.* **2004**, *126*, 10224−10225.
(37) Wulff, G. *Z. Kristallogr. - Cryst. Mater.* **1901**, *34*, 449−530.
(38) Auyeung, E.; Li, T. I. N. G.; Senesi, A. J.; Schmucker, A. L.; Pals, B. C.; de la Cruz, M. O.; Mirkin, C. A. *Nature* **2014**, *505*, 73−77.
(39) Douglas, J. F.; Roovers, J.; Freed, K. F. *Macromolecules* **1990**, *23*, 4168−4180.
(40) Ziherl, P.; Kamien, R. D. *Phys. Rev. Lett.* **2000**, *85*, 3528−3531.
(41) Koch, C.; Panagiotopoulos, A. Z.; Lo Verso, F.; Likos, C. N. *Soft Matter* **2013**, *9*, 7424−7436.
(42) Capone, B.; Coluzza, I.; LoVerso, F.; Likos, C. N.; Blaak, R. *Phys. Rev. Lett.* **2012**, *109*, 238301.
(43) Roh, Y. H.; Lee, J. B.; Kiatwuthinon, P.; Hartman, M. R.; Cha, J. J.; Um, S. H.; Muller, D. A.; Luo, D. *Small* **2011**, *7*, 74−78.
(44) Bianchi, E.; Largo, J.; Tartaglia, P.; Zaccarelli, E.; Sciortino, F. *Phys. Rev. Lett.* **2006**, *97*, 168301.
(45) Anderson, V. J.; Lekkerkerker, H. N. W. *Nature* **2002**, *416*, 811−815.
(46) Auyeung, E.; MacFarlane, R. J.; Choi, C. H. J.; Cutler, J. I.; Mirkin, C. A. *Adv. Mater.* **2012**, *24*, 5181−5186.

DOI: 10.1021/acs.nanolett.7b00980
Nano Lett. 2017, 17, 3276−3281